UNITED NATIONS EDUCATIONAL, SCIENTIFIC AND CULTURAL ORGANIZATION
INTERNATIONAL ATOMIC ENERGY AGENCY
INTERNATIONAL CENTRE FOR THEORETICAL PHYSICS
I.C.T.P., P.O. BOX 586, 34100 TRIESTE, ITALY, CABLE: CENTRATOM TRIESTE

H4.SMR/1011 - 7

Fourth Workshop on Non-Linear Dynamics
and Earthquake Prediction

6 - 24 October 1997

Self-Organized Criticality

D. L. TURCOTTE

Cornell University
Institute for the Study of the Continents
Dept. of Geological Scientists
Ithaca, New York, U.S.A.

Chapter Sixteen

SELF-ORGANIZED CRITICALITY

16.1 Sand-pile models

In the last chapter we considered the renormalization group method for treating large interactive systems. By assuming scale invariance a relatively small system could be scaled upward to a large interactive system. The approach is often applicable to systems that have critical point phenomena. In this chapter we consider the alternative approach to large interactive systems. This approach is called self-organized criticality. A system is said to be in a state of self-organized critically if it is maintained near a critical point (Bak *et al.*, 1988). According to this concept a natural system is in a marginally stable state: when perturbed from this state it will evolve naturally back to the state of marginal stability. In the critical state there is no longer a natural length scale so that fractal statistics are applicable.

The simplest physical model for self-organized criticality is a sand pile. Consider a pile of sand on a circular table. Grains of sand are randomly dropped on the pile until the slope of the pile reaches the critical angle of repose. This is the maximum slope that a granular material can maintain without additional grains sliding down the slope. One hypothesis for the behavior of the sand pile would be that individual grains could be added until the slope is everywhere at an angle of repose. Additional grains would then simply slide down the slope. This is not what happens. The sand pile never reaches the hypothetical critical state. As the critical state is approached additional sand grains trigger landslides of various sizes. The frequency–size distribution of landslides is fractal. The sand pile is said to be in a state of self-organized criticality. On average the number of sand grains added balances the number that slide down the slope and off the table. But the actual number of grains on the table fluctuates continuously.

The principles of self-organized criticality are illustrated using a simple cellular-automata model. As in the previous chapter we again consider a square grid of n boxes. Particles are added to and lost from the grid using the following procedure.

(1) A particle is randomly added to one of the boxes. Each box on the grid is assigned a number and a random-number generator is used to determine the box to which a particle is added. This is a statistical model.

(2) When a box has four particles it is unstable and the four particles are redistributed to the four adjacent boxes. If there is no adjacent box the particle is lost from the grid. Redistributions from edge boxes result in the loss of one particle from the grid. Redistributions from the corner boxes result in the loss of two particles from the grid.

(3) If after a redistribution of particles from a box any of the adjacent boxes has four or more particles, it is unstable and one or more further redistributions must be carried out. Multiple events are common occurrences for large grids.

(4) The system is in a state of marginal stability. On average, added particles must be lost from the sides of the grid.

This is a nearest neighbor model. At any one step a box interacts only with its four immediate neighbors. However, in a multiple event interactions can spread over a large fraction of the grid.

The behavior of the system is characterized by the statistical frequency–size distribution of events. The size of a multiple event can be quantified in several ways. One measure is the number of boxes that become unstable in a multiple event. Another measure is the number of particles lost from the grid during a multiple event.

When particles are first added to the grid there are no redistributions and no particles are lost from the grid. Eventually the system reaches a quasi-equilibrium state. On average the number of particles lost from the edges of the grid is equal to the number of particles added. Initially, small redistribution events dominate, but in the quasi-equilibrium state the frequency–size distribution is fractal. This is the state of self-organized criticality. There is a strong resemblance to the renormalization group approach considered in the last chapter. In the renormalization group approach the frequency–size statistics are fractal only at the critical point. In the cellular automata model the frequency–size statistics are fractal only in the state of self-organized criticality.

The behavior of a sand pile and the behavior of the cellular automata model have remarkable similarities to the seismicity associated with an active tectonic zone. The addition of particles to the grid is analogous to the addition of stress caused by the relative displacement between two surface plates, say, across the San Andreas fault. The multiple events in which particles are transferred and are lost from the grid are analogous to earthquakes in which some accumulated stress is transferred and some is lost. There is a strong similarity between the frequency–magnitude statistics of multiple events and the Gutenberg–Richter statistics for earthquakes. Before consid-

ering the analogy further, we will describe the behavior of the cellular automata model in some detail.

As a specific example we consider the 3×3 grid illustrated in Figure 16.1. The nine boxes are numbered sequentially from left to right and top to bottom as illustrated in Figure 16.1(a). The cellular automata model has been run for some time to establish a state of self-organized criticality. The further evolution of the model is as follows and is illustrated in Figure 16.1(b).

Step 1 A particle has been randomly added to box 8. The number of particles in this box has been increased from two to three.

Step 2 A particle has been randomly added to box 6, increasing the number of particles from one to two. This addition is illustrated in the change between steps 1 and 2 in Figure 16.1(b).

Step 3a A particle has been randomly added to box 5, increasing the number of particles from three to four and making it unstable; the four particles are redistributed to the four adjacent boxes, increasing the number of particles in box 2 from three to four, the number of particles in box 4 from three to four, the number of particles in box 6 from two to three, and the number of particles in box 8 from three to four. Boxes 2, 4, and 8 are now unstable. No particles are lost from the

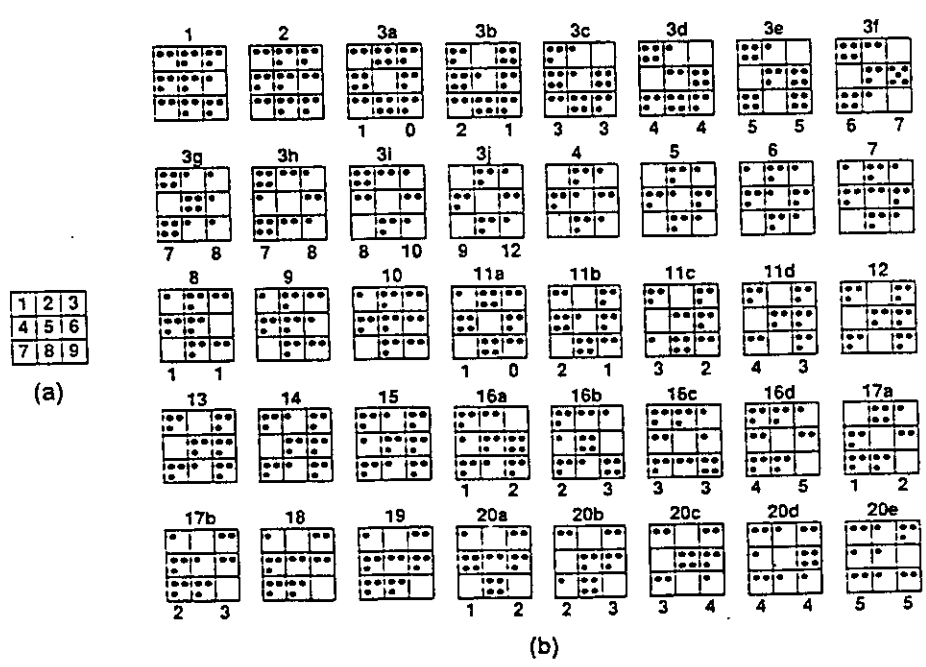

Figure 16.1. Illustration of the cellular automata model for a 3×3 grid of boxes. The boxes are numbered 1 to 9 as shown in (a). Particles are randomly added to boxes in (b) as shown in steps 1 and 2. In step 3a an added particle in box 5 gives four particles and these are redistributed to the adjacent boxes. Nine more redistributions are required in steps 3b to 3j before the grid is stabilized. The first number below the grid is the number of boxes that have been unstable in the sequence of redistributions. The second number is the cumulative number of particles that have been lost from the grid in the sequence of redistributions.

grid. This redistribution is illustrated in step 3a in Figure 16.1(b). The numbers below the grid are, on the left, the cumulative numbers of boxes subject to redistribution and, on the right, the cumulative number of particles lost from the grid.

Step 3b Since several boxes are now unstable, an arbitrary choice must be made about which box will be considered first for further redistribution. The choice does not have a significant effect on the statistical evolution of the system. The four particles in box 2 are redistributed. One is lost from the grid and box 3 becomes unstable with four particles. Boxes 3, 4, and 8 remain unstable. In this sequence of redistributions two boxes have been made unstable and one particle has been lost from the grid.

Step 3c The four particles in box 3 are redistributed. Two are lost from the grid and box 6 becomes unstable with four particles. Boxes 4, 6, and 8 remain unstable. In this sequence of redistributions three boxes have been made unstable and three particles have been lost from the grid.

Step 3d The four particles in box 4 are redistributed. One is lost from the grid and box 1 becomes unstable with four particles. Boxes 1, 6, and 8 remain unstable. In this sequence of redistributions four boxes have been made unstable and four particles have been lost from the grid.

Step 3e The four particles on grid point 8 are redistributed. One is lost from the grid and boxes 7 and 9 become unstable with four particles. Boxes 1, 6, 7, and 9 remain unstable. In this sequence of redistributions five boxes have been made unstable and five particles have been lost from the grid.

Step 3f The four particles in box 9 are redistributed. Two are lost from the grid and box 6 is now unstable with five particles. Grid points 1, 6, and 7 remain unstable. In this sequence of redistributions six boxes have been made unstable and seven particles have been lost from the grid.

Step 3g Four of the five particles in box 6 are redistributed. One is lost from the grid and box 5 is now unstable. Boxes 1, 5, and 7 remain unstable. In this sequence of redistributions seven boxes have been made unstable and eight particles have been lost from the grid.

Step 3h The four particles in box 5 are redistributed for the second time. No particles are lost and no boxes are made unstable. Boxes 1 and 7 remain unstable. In this sequence of redistributions seven boxes have been made unstable and eight particles have been lost from the grid.

Step 3i The four particles in box 7 are redistributed and two are lost from the grid. No boxes are made unstable so that 1 is the only remaining unstable box. In this sequence of redistributions eight boxes have been made unstable and ten particles have been lost from the grid.

Step 3j The four particles in box 1 are redistributed and two are lost from the grid. No boxes remain unstable so that the sequence of 10 redistributions has completed step 3. During step 3 all nine boxes were unstable and 12 particles were lost from the grid.

Step 4 A particle has been randomly added to box 5, increasing the number of particles from zero to one.

Step 5 A particle has been randomly added to box 6, increasing the number of particles from two to three.

This relatively simple example illustrates how the cellular automata model works. To develop significant statistics larger grids must be considered. Kadanoff *et al.* (1989) have carried out extensive studies of the behavior of this model as a function of grid size. One statistical measure of the size of an event is the number of grid points that become unstable. The results for a 50×50 grid of boxes are given in Figure 16.2. The number of events N in which a specified number of boxes A participated is given as a function of the number of boxes. A good correlation with a fractal power law is obtained, with a slope of 1.03. Since the number of grid points is equivalent to an area, the equivalent fractal dimension is $D = 2.06$. This statistical behavior appears to resemble that of distributed seismicity. However, the statistics in Figure 16.2 are not cumulative. In fact a fractal relation is not obtained for the cumulative statistics.

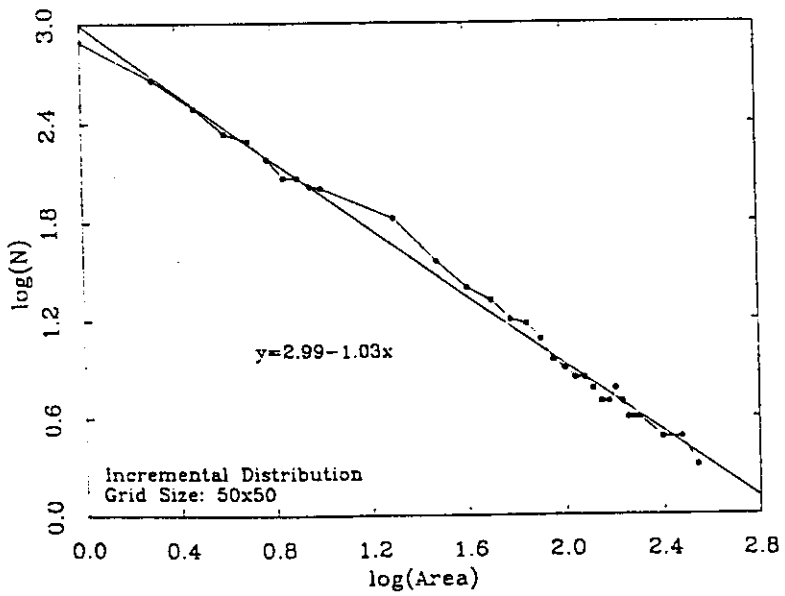

Figure 16.2. Statistics for a cellular-automata model on a 50×50 grid. The number N of events in which a specified number A of boxes became unstable is given as a function of A.

A number of groups have studied the frequency–size statistics of avalanches on real sand piles, and in some cases fractal distributions have been found (Evesque, 1991; Nagel, 1992; Puhl, 1992). Held *et al.* (1990) found fractal statistics applicable for small avalanches but not for large avalanches. Bretz *et al.* (1992) and Rosendahl *et al.* (1993) found near-periodic large avalanches and a fractal distribution of small avalanches. Segre and Deangeli (1995) have developed a more realistic cellular-automata model for actual landslides. The fractal statistics of actual landslides have been considered by Yokoi *et al.* (1995).

Turbidite deposits are associated with slumps off the continental margin. These avalanche-like events can be considered a natural analog for sand slides and thus for the cellular-automata model considered above. Turbidite deposits are generally composed of a sequence of layers, each layer representing a distinct event (slump). Each layer is composed of an upward gradation from coarse-grained sediments to fine-grained sediments, and individual layers are generally separated by well-defined bedding planes.

Several studies of the thickness statistics of turbidite deposits have been carried out. Rothman *et al.* (1994) carried out direct measurements on an outcrop of the Kingston Peak Formation near the southern end of Death Valley, California. Their results are given in Figure 16.3(a); an excellent correlation with the fractal relation (2.6) is obtained taking $D = 1.39$. Hiscott *et al.* (1992) have studied a volcaniclastic turbidity deposit in the Izu–Bonin forearc basin off the shore of Japan. Layer thicknesses were obtained from formation-microscanner images from well logs in the middle to upper Oligocene part of the section. Results for two DSDP holes located 75 km apart are given in Figure 16.3(b): a good correlation with (2.6) is obtained taking $D = 1.12$.

It is difficult to make a direct comparison between the thickness statistics of the sedimentary layers and the volume statistics of sand piles. However, the layer statistics appear to be scale invariant to a good approximation. It is interesting to note that the fractal dimensions of the thickness statistics are greater than one. For such a one-dimensional sequence it would appear that this would be impossible considering the examples given in Figure 2.1.

The constructions illustrated in Figure 16.4 show that D can in fact be greater than one. The standard Cantor set is illustrated in Figure 16.4(a): one layer, $N_1 = 1$, with thickness $r_1 = \frac{1}{3}$, two layers, $N_2 = 2$, with thickness $r_2 = \frac{1}{9}$, four layers, $N_3 = 4$, with thickness $r_3 = \frac{1}{27}$. From (2.1) $D = \ln 2/\ln 3 = 0.6309$. In Figure 16.4(b) a stretched Cantor set is illustrated. At each step the remaining segments are stretched by a factor of two before being further subdivided. This gives $N_1 = 1$ with $r_1 = \frac{1}{3}$, $N_2 = 2$ with $r_2 = \frac{2}{9}$, $N_3 = 4$ with $r_3 = \frac{4}{27}$. From (2.1) $D = \ln 2/\ln (3/2) = 1.710$. The length L of the set is unbounded. $L \to \infty$ as $r \to 0$. For real data sets with both upper and lower bounds on r, this construction illustrates that values of D greater than one are acceptable.

To model crustal seismicity, Barriere and Turcotte (1994) introduced a cellular-automata model in which the boxes have a scale-invariant distribution of sizes. The objective was to model a scale-invariant distribution of fault sizes. When a redistribution from a box occurs, it is equivalent to a characteristic earthquake on the fault. A redistribution from a small box (a

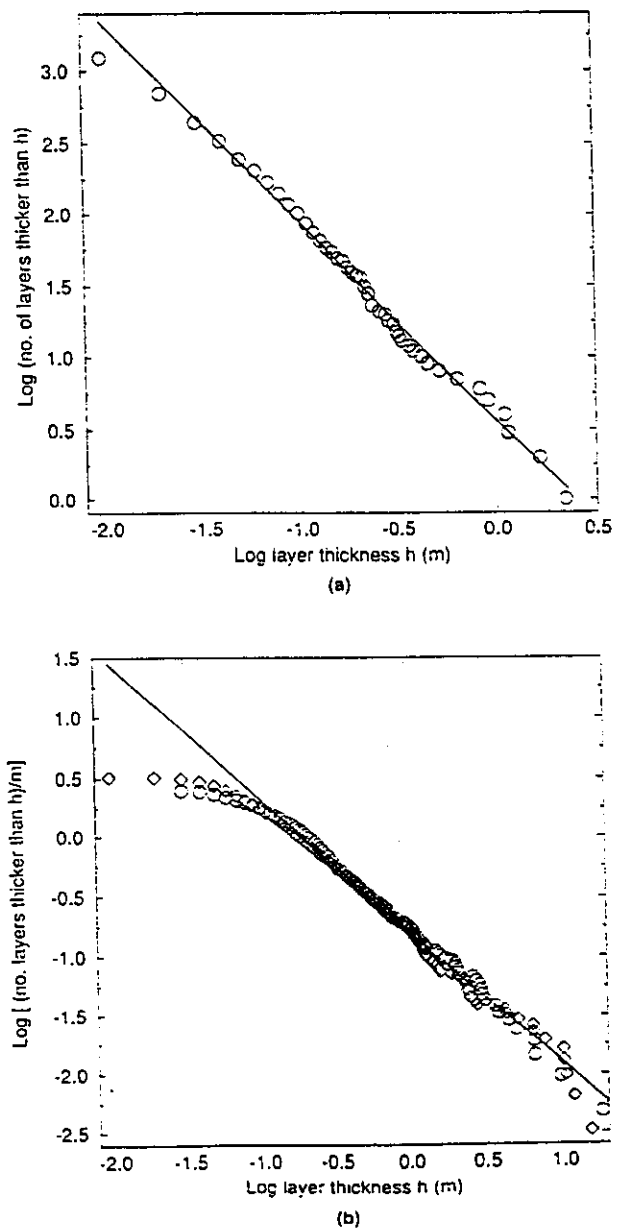

Figure 16.3. Cumulative frequency–thickness statistics for turbidite sequences of sedimentary layers. (a) Kingston Peak Formation near the southern end of Death Valley, CA. (b) Izu–Bonin forearc basin off the shore of Japan. The roll-off for thin layers is attributed to loss of resolution. The straight-line correlations with the fractal relation (2.6) give $D = 1.39$ in (a) and $D = 1.12$ in (b).

foreshock) may trigger an instability in a large box (the main shock). A redistribution from a large box always triggers many instabilities in the smaller boxes (aftershocks).

As a specific example we again consider the surface exposure of the fractal fragmentation model given in Figure 3.3. A fifth-order realization of this construction is given in Figure 16.5. We have $N_1 = 1$ box with $r_1 = \frac{h}{2}$, $N_2 = 3$ boxes with $r_2 = \frac{h}{4}$, $N_3 = 9$ boxes with $r_3 = \frac{h}{8}$, $N_4 = 27$ boxes with $r_4 = \frac{h}{16}$, and $N_5 = 108$ boxes with $r_5 = \frac{h}{32}$. Except for N_5 the N_i are related to the r_i by the fractal relation (2.1) with $D = \ln 3/\ln 2 = 1.5850$.

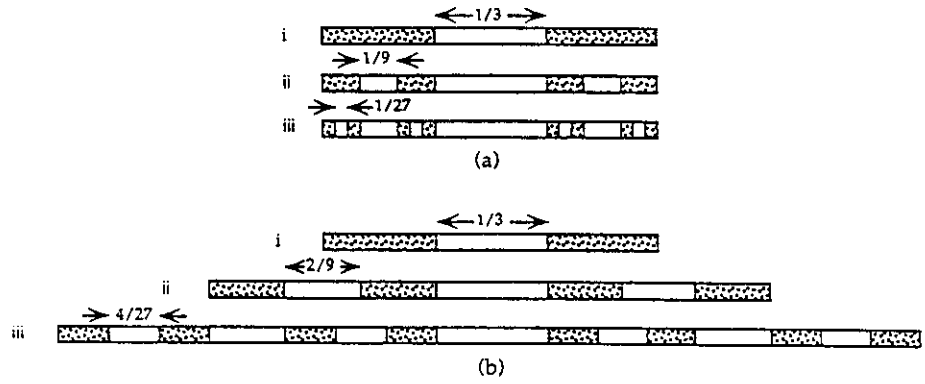

Figure 16.4. (a) Cantor set $N_1 = 1$, $r_1 = \frac{1}{3}$; $N_2 = 2$, $r_2 = \frac{1}{9}$; $N_3 = 4$, $r_3 = \frac{1}{27}$; $D = \ln 2/\ln 3 = 0.6309$. (b) Stretched Cantor set $N_1 = 1$, $r_1 = \frac{1}{3}$; $N_2 = 2$, $r_2 = \frac{2}{9}$, $N_3 = 4$, $r_3 = \frac{4}{27}$; $D = \ln 2/\ln (3/2) = 1.710$.

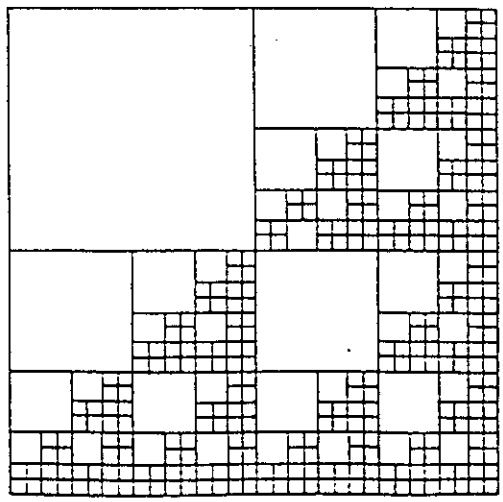

Figure 16.5. Illustration of the fractal cellular model corresponding to the discrete model for comminution illustrated in Figure 3.7 carried to fifth order. $D = \ln 3/\ln 2 = 1.585$.

The standard cellular-automata rules are applied to this model:

(1) Particles are added one at a time to randomly selected boxes. The probability that a particle is added to a box is proportional to the area $A_i = r_i^2$ of the box.
(2) A box becomes unstable when it contains $4A_i$ particles.
(3) Particles are redistributed to immediately adjacent boxes or are lost from the grid. The number of particles redistributed to an adjacent box is proportional to the linear dimension r_i of that box.
(4) If, after a redistribution of particles from a box, any of the adjacent boxes are unstable, one or more further redistributions are carried out. In any redistribution, the critical number of particles is redistributed. Redistributions are continued until all boxes are stable.

The cumulative frequency–magnitude statistics for main shocks of a seventh-order (128 × 128) version of the model are given in Figure 16.6. We find an excellent correlation with the fractal relation (2.6) taking $D = 2.50$ ($b = 1.25$). This is significantly higher than the observed values for distributed seismicity. Evernden (1970) has obtained b-values for regional seismicity and concludes that $b = 0.85 \pm 0.20$. It was also found that 31.5% of the largest events had foreshocks. This is in reasonable agreement with studies of actual earthquakes; von Seggern *et al.* (1981) found that 21% of the earthquakes studied had foreshocks and Jones and Molnar (1979) found that 44%

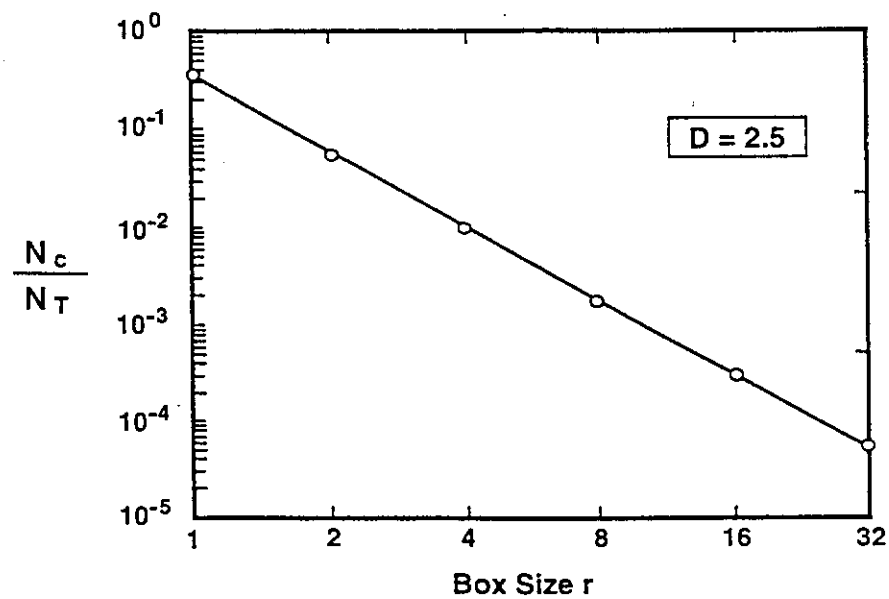

Figure 16.6. Cumulative frequency–magnitude statistics for unstable events. The number of events N_c in boxes equal to or smaller than r is divided by the total number of events N_T and given as a function of r. The correlation is with (2.6) taking $D = 2.5$.

of larger shallow earthquakes that could be recorded teleseismically had foreshocks. The aftershocks also correlate well with (2.6) taking $D = 2.02$ ($b = 1.01$). A similar model has been proposed by Henderson *et al.* (1994).

16.2 Slider-block models

Slider-block models that exhibit self-organized criticality can also be constructed. In Chapter 11 we showed that a pair of interacting slider blocks can exhibit deterministic chaos. This model is easily extended to include large numbers of slider blocks. Carlson and Langer (1989) considered long linear arrays of slider blocks with each block connected by springs to the two neighboring blocks and to a constant-velocity driver. They used a velocity-weakening friction law and considered up to 400 blocks. Slip events involving large numbers of blocks were observed, the motion of all blocks involved in a slip event were coupled, and the applicable equations of motion had to be solved simultaneously. Although the system is completely deterministic, the behavior was apparently chaotic. Frequency–size statistics were obtained for slip events and the events fell into two groups: smaller events obeyed a power-law (fractal) relationship but there was an anomalously large number of large events that included all the slider blocks. This model was considered to be a model for the behavior of a single fault, not a model for distributed seismicity. The large events were associated with characteristic earthquakes on the fault and smaller events with background seismicity on the fault between characteristic earthquakes.

Nakanishi (1990, 1991) proposed a model that combined features of the cellular-automata model and the slider-block model. A linear array of slider blocks was considered but only one block was allowed to move in a slip event. The slip of one block could lead to the instability of either or both of the adjacent blocks, which would then be allowed to slip in a subsequent step or steps, until all blocks were again stable. Brown *et al.* (1991) proposed a modification of this model involving a two-dimensional array of blocks. Other models of this type have been considered by Bak and Tang (1989), Takayasu and Matsuzaki (1988), Ito and Matsuzaki (1990), Sornette and Sornette (1989, 1990), Langer and Tang (1991), Carlson (1991a, b), Carlson *et al.* (1991, 1993a, b, 1994), Matsuzaki and Takayasu (1991), Rundle and Brown (1991), Feder and Feder (1991), Chen *et al.* (1991), Shaw *et al.* (1992), Huang *et al.* (1992), Christensen and Olami (1992), Olami and Christensen (1992), Olami *et al.* (1992), Vasconcelos *et al.* (1992), de Sousa Vieira (1992), Cowie *et al.* (1993), Shaw (1993a, b, 1994, 1995), Rundle and Klein (1993, 1995), de Sousa Vieira *et al.* (1993), Schmittbuhl *et al.* (1993), Knopoff *et al.* (1993), Ding and Yu (1993), Lu *et al.* (1994), Senatorski (1994), Xu and Knopoff (1994), Pepke and Carlson (1994), Pepke *et al.*

(1994), Rubio and Galeano (1994), Robinson (1994), Espanol (1994), and Lin and Taylor (1994). McCloskey (1993), and McCloskey and Bean (1994) considered arrays of slider blocks connected to two driver plates, and these driver plates were treated as a pair of interacting slider blocks.

The standard two-dimensional array of slider blocks is illustrated in Figure 16.7. In the cellular-automata approximation it is assumed that during the sliding of one block, all other blocks are stationary; this requirement limits the system to nearest neighbor interactions, which is characteristic of cellular-automata systems. To minimize the complexity we considered a discontinuous static–dynamic friction law. After non-dimensionalization of the governing equations, the governing parameters are $\alpha = k_c/k_l$ (k_c is the spring constant of the connector springs, k_l is the spring constant of the puller springs), α is a measure of the stiffness of the system, $\phi = F_s/F_d$ (the ratio of the static friction F_s to dynamic friction F_d), and N the number of blocks considered. In this model the parameter ϕ can be eliminated by rescaling. Thus for large systems (N very large) the only scaling parameter is the stiffness α. Frequency–size statistics for a 50×50 ($N = 2500$) array are given in Figure 16.8 for several values of the stiffness parameter α. A good correlation is obtained with the fractal relation (2.6) with $D = 2.72$. The frequency–size relation shows a roll-off from the power law near the larger end of the scaling region. This deviation is reduced as the parameter α increases. Frequency–size statistics for several different size arrays are given in Figure 16.9. When the parameter $\alpha/N^{1/2}$ is greater than one, we observe an excess number of catastrophic events that include the failure of all blocks. The failure statistics of these multiple-block systems clearly indicate a self-organized critical behavior and are remarkably similar to distributed seismicity.

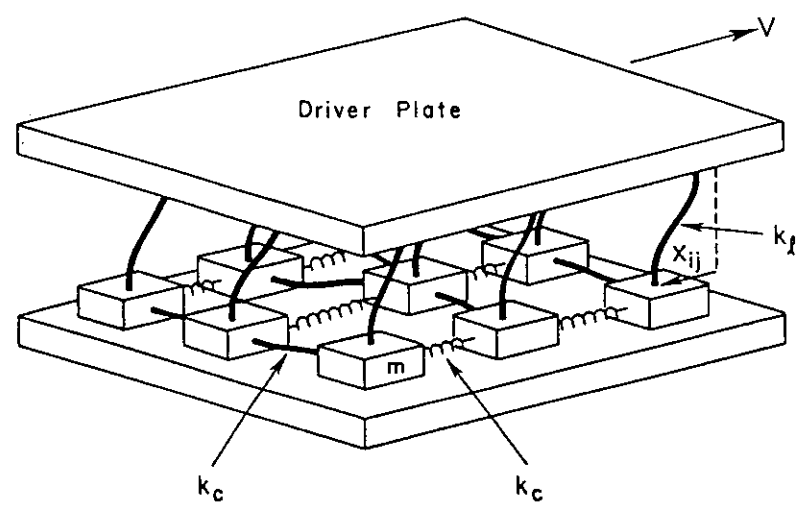

Figure 16.7. Illustration of the two-dimensional slider block model. An array of blocks each with mass m is pulled across a surface by a driver plate at a constant velocity V. Each block is coupled to the adjacent blocks with either leaf or coil springs with constant k_c, and to the driver plate with leaf springs with spring constant k_l. The extension of the (i, j) pulling spring is x_{ij}.

The frequency–size distribution of events associated with self-organized criticality certainly resembles the regional distribution of earthquakes in a zone of active tectonics. This suggests that interactions between faults play an essential role in the behavior of such zones.

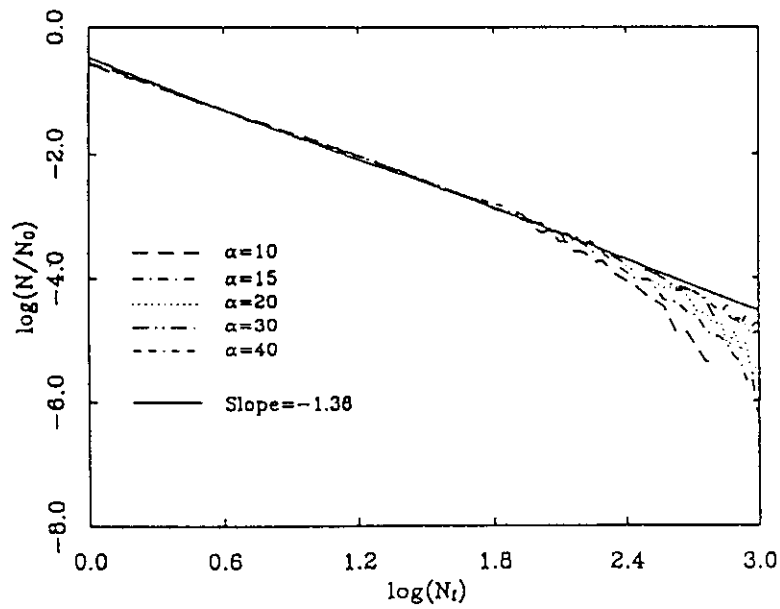

Figure 16.8. The ratio of the number of events N with size N_f to the total number of events N_0 is plotted against N_f (N_f is the number of blocks that participate in an event and is a measure of the area of an event). Results are given for $\phi = 1.5$ and $\alpha = 10$, 15, 20, 30, and 40. The solid line is the correlation with the power-law (fractal) relation (2.6); the corresponding fractal dimension is $D = 2.72$.

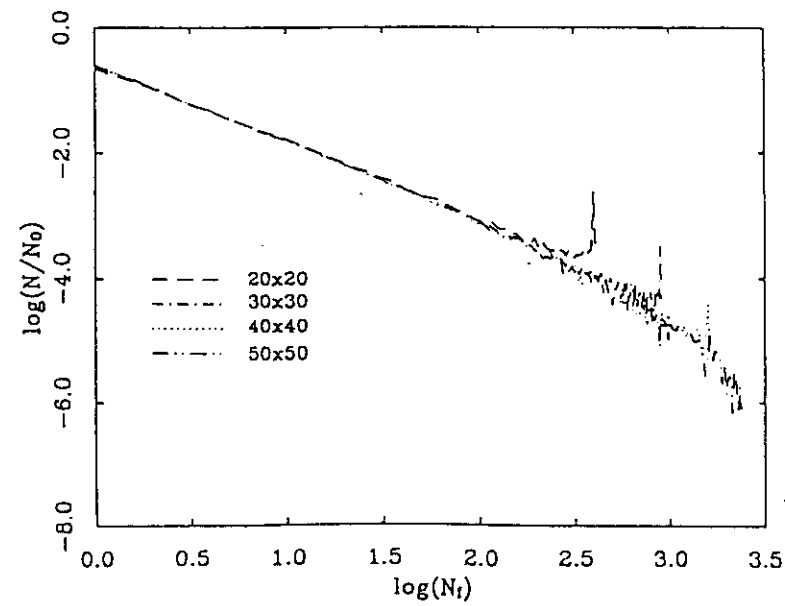

Figure 16.9. The ratio of the number of events N with size N_f to the total number of events N_0 is plotted against N_f. Results are given for systems of size 20×20, 30×30, 40×40, and 50×50 with parameters $\phi = 1.5$ and $\alpha = 50$. The peaks at log $N_f = 2.60$, 2.95, and 3.20 correspond to catastrophic events involving the entire system.

An important consequence of a critical state in the crust is the large range of interactions. A basic question is whether an earthquake on one part of the planet, say Mexico, is correlated with an earthquake at a large distance, say Japan. The classical approach to earthquakes would say that this is impossible. The stresses associated with seismic waves are too small to trigger an earthquake and there is no conclusive observational evidence for correlated events on this spatial scale. The stress changes associated with the fault displacement are localized and are damped by the athenospheric viscosity. However, interactions at large distances are a characteristic of critical phenomena. The interactions are not through the direct transmission of stress but through the interactions of faults with each other. Scholz (1991) has argued that the entire earth's crust is in a state of self-organized criticality. He sites as direct supporting evidence the induced seismicity associated with dams and other sources. Whenever a reservoir is filled behind a large new dam, extensive swarms of earthquakes are generally triggered. This is evidence that the crust is at the brink of failure even at large distances from plate boundaries.

This action at a distance may help to explain the apparent success of the earthquake-prediction algorithms developed at the International Institute for the Theory of Earthquake Prediction and Theoretical Geophysics in Moscow under the direction of Academician V. I. Keilis-Borok. This approach is based on pattern recognition of distributed regional seismicity (Keilis-Borok, 1990; Keilis-Borok and Rotwain, 1990; Keilis-Borok and Kossobokov, 1990). The pattern recognition includes quiescence (Schreider, 1990), increases in the clustering of events, and changes in aftershock statistics (Molchan *et al.*, 1990). In reviewing regional seismicity after a major earthquake it is often observed that the regional seismicity in the vicinity of the fault rupture was anomalously low for several years prior to the earthquake (Kanamori, 1981; Wyss and Haberman, 1988). This is known as seismic quiescence. The problem has been to provide quantitative measures of quiescence prior to the major earthquake. We discussed the fractal clustering of earthquakes in Chapter 6. The clustering of regional seismicity appears to become more fractal-like prior to a large earthquake. There also appears to be a systematic reduction in the number of aftershocks associated with regional intermediate-sized earthquakes prior to a major earthquake. Pattern-recognition algorithms were developed to search earthquake catalogs for anomalous recursory behavior. Premonitory seismicity patterns were found for strong earthquakes in California and Nevada (algorithm "CN") and for earthquakes with $M > 8$ worldwide (algorithm "M8"). When a threshold of the anomalous behavior was reached, a warning of the time of increased probability (TIP) of an earthquake was issued.

On a worldwide basis TIPs were triggered prior to 42 of 47 events. TIPS were released prior to the Armenian earthquake on December 7, 1988, and to

the Loma Prieta earthquake on October 17, 1989. These are illustrated in Figure 16.10. The TIP issued for region 3 in the Caucasus during January 1987 was still in effect when the Armenian earthquake occurred in this region on December 7, 1988. TIPS were issued for region 5 in California during October 1984 and for region 6 during January 1985. These warnings were still in effect when the Loma Prieta earthquake occurred within these overlapping regions on October 17, 1989.

The fault rupture of the Loma Prieta earthquake extended over about 40 km. However, the prediction algorithms detected anomalous seismic behavior over two regions with diameters of 500 km. Self-organized criticality can explain anomalous correlated behavior over large distances.

This approach is certainly not without its critics. Independent studies have established the validity of the TIP for the Loma Prieta earthquake; however, the occurrence of recognizable precursory patterns prior to the Landers earthquake are questionable. Also, the statistical significance of the size and time intervals of warnings in active seismic areas has been questioned. Nevertheless, seismic activation prior to a major earthquake certainly appears to be one of the most promising approaches to earthquake prediction.

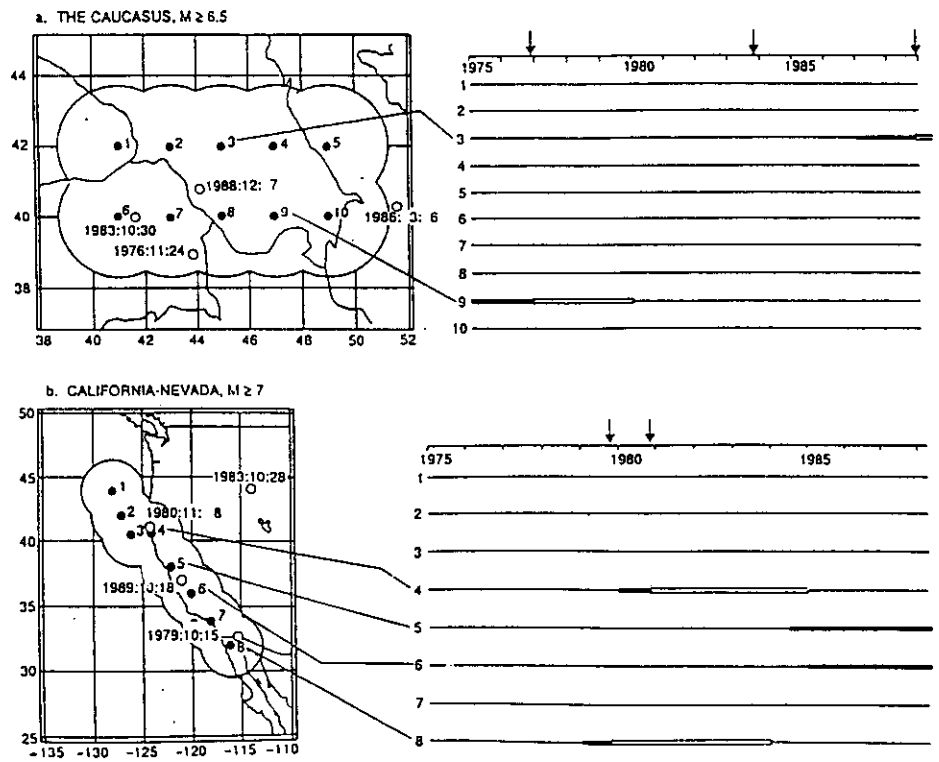

Figure 16.10. Illustrations of the Armenian (December 7, 1988) and Loma Prieta (October 18, 1989, Moscow time) earthquakes by Keilis-Borok (1990). In (a) the Caucasus region is broken up into 10 areas with diameters of 500 km; two warnings (for region 3 and 9) are shown on the right. The locations and times of four earthquakes are also given. In (b) the California–Nevada region is broken up into eight areas with diameters of 500 km. Four warnings (for regions 4–6, 8) and the locations and times of four earthquakes are given.

Although long-distance correlations between earthquakes are a subject of considerable controversy, such correlations have been widely accepted in China and Russia (as well as the former Soviet Union). A striking example was a sequence of five earthquakes that occurred in China between 1966 and 1976. These were the $m = 7.2$ Shentai (1966), $m = 6.3$ Hijien (1967), $m = 7.4$ Bo Sea (1969), $m = 7.3$ Haicheng (1975), and the $m = 7.8$ Tangshan (1976) earthquakes. These earthquakes spanned a distance of some 700 km, and the Haicheng earthquake was successfully predicted by the Chinese, at least partially on the basis of seismic activation (Scholz, 1977). However, the Tangshan earthquake was not predicted and estimates of fatalities in this earthquake range from 250,000 to 450,000.

Seismic activation has been previously recognized in association with an increase in seismicity that occurred in the San Francisco Bay area prior to the 1906 earthquake (Sykes and Jaumé, 1990). Earthquakes with estimated magnitudes between 6.5 and 7.0 occurred in 1865 (Santa Cruz Mountains), 1868 (Hayward), 1892 (Vacaville), and 1898 (Mare Island). There is a serious concern that a similar seismic activation is now underway in southern California. A number of intermediate-size earthquakes have occurred in southern California in the last 45 years. These include the $m = 7.4$ Kern County earthquake on July 21, 1952, the $m = 6.4$ San Fernando earthquake on February 9, 1971, the $m = 7.6$ Landers earthquake on June 28, 1992, and the $m = 6.6$ Northridge earthquake on January 17, 1994.

The Landers earthquake provided direct evidence that faults interact with each other over large distances (Hill *et al.*, 1993). The Landers earthquake triggered earthquakes at 14 distant sites scattered over the western United States. The farthest site was Yellowstone National Park in Wyoming, 1250 km from Landers. Just how information is transmitted over these distances is uncertain. One hypothesis is that the surface waves of the Landers earthquake were responsible. However, the stress levels associated with surface waves at this distance are no larger than the daily variations in stress associated with the earth tides.

It is known from statistical mechanics that near a critical point spatial correlations extend to large distances. To better understand the statistical mechanics of slider-block models, we consider a two-dimensional array of slider blocks without a driver plate. Each block is connected to its four neighbors with springs (spring constant k) and is confined to move in the x-direction. The slider blocks interact frictionally with a surface; however, to conserve energy the dynamic friction is assumed to be zero. The problem is specified by the static friction and the initial total energy in the system. The force on a block (i, j) is

$$F_{i,j} = k\,(x_{i,j-1} + x_{i,j+1} + x_{i-1,j} + x_{i+1,j} - 4x_{i,j}) \tag{16.1}$$

A block slides if $|F_{i,j}| > F_s$, where F_s is the prescribed static friction force. To simplify the analysis and simulations, only one block in the array is updated during each microscopic time step. Before the update there are two possible states:

(1) The block was stuck after the previous update $|F_{i,j}|_{n+} < F_s$. However, the forces on the block have changed because of subsequent updates on neighboring blocks, there are now two possibilities:
   (a) The block is still stable, $|F_{i,j}|_{n+1-} < F_s$, and the update is terminated.
   (b) The block is still unstable, $|F_{i,j}|_{n+1-} > F_s$. In this case motion of the single slider block is given by

$$m\frac{d^2x_{i,j}}{dt^2} - F_{i,j} = 0 \tag{16.2}$$

The slipping block executes one-half of an harmonic cycle and sticks when the velocity is again zero. The change in the position of block (i, j), $\Delta x_{i,j}$, is related to the initial force on the block $(F^0_{i,j})_{n+1-}$ by

$$\Delta x_{i,j} = \frac{(F_{i,j})_{n+1-}}{2k} \tag{16.3}$$

The new net force on the block $(F_{i,j})_{n+1+}$ is determined, again there are two possibilities:
   (i) If $|F_{i,j}|_{n+1+} < F_s$ the block remains stuck until the next update,
   (ii) If $|F_{i,j}|_{n+1+} > F_s$ the block slips until the next update.

(2) The block was slipping after the previous update $|F_{i,j}|_{n+} > F_s$. But again the forces on the block have changed because of subsequent updates on neighboring blocks. There are two possibilities:
   (a) The block is now stable, $|F_{i,j}|_{n+1-} < F_s$, and the step is terminated.
   (b) The block is still unstable $|F_{i,j}|_{n+1-} > F_s$, and then (16.3) is used to determine the new position of the block and the new net force on the block $(F_{i,j})_{n+1+}$ is determined. Again there are two possibilities:
      (i) If $|F_{i,j}|_{n+1+} < F_s$ the block remains stuck until the next update.
      (ii) If $|F_{i,j}|_{n+1+} > F_s$, the block slips until the next update.

The slider blocks are considered sequentially using a checker-board algorithm to sweep across the two-dimensional array.

It is convenient to introduce the nondimensional variables $\bar{F}_{i,j} = F_{i,j}/F_s$, $\bar{x} = kx/F_s$, $\bar{t} = t\sqrt{k/m}$, and $\bar{E}_k = kE_k/F_s^2$ where E_k is the energy in spring k. The nondimensional force on a block is

$$\bar{F}_{i,j} = \bar{x}_{i,j-1} + \bar{x}_{i,j+1} + \bar{x}_{i-1,j} + \bar{x}_{i+1,j} - 4\bar{x}_{i,j} \tag{16.4}$$

and the motion of a block is given by

$$\frac{d^2\bar{x}_{i,j}}{d\bar{t}^2} - \bar{F}_{i,j} = 0 \tag{16.5}$$

If $|\bar{F}_{ij}|_- > 1$, block (i, j) is unstable and its nondimensional slip is given by

$$\Delta\bar{x}_{ij} = \frac{1}{2}\bar{F}_{ij-} \tag{16.6}$$

At $t = 0$ the blocks are given a random distribution of displacements of the nondimensional energy in spring k is $\bar{E}_k$. The only parameter in this problem is the mean energy per spring introduced at $t = 0$, E, which is given by

$$E = \langle \bar{E}_k \rangle \tag{16.7}$$

Since no energy is dissipated, this value remains constant and we use it as a control parameter for the model. If E is large, very few blocks will stick and we would expect that the system should behave like a set of harmonic oscillators with a Maxwell–Boltzmann (Gaussian) distribution of displacements.

If the distribution of displacements of individual block (i, j) is Gaussian, the distribution of spring displacements will also be Gaussian. If this is the case, the probability distribution function for the energies in the springs $\bar{E}_k$ will be given by

$$p(\bar{E}_k) = \frac{\exp\left(-\dfrac{\bar{E}_k}{2E}\right)}{\sqrt{2\pi E\bar{E}_k}} \tag{16.8}$$

One of the questions we address is whether the system evolves to this Maxwell–Boltzmann distribution. The corresponding probability distribution function for the forces on the springs is

$$p(\bar{F}_k) = \frac{\exp\left(-\frac{\bar{F}_k^2}{4E}\right)}{2\sqrt{\pi E}} \tag{16.9}$$

However, the slip condition for a block is determined by the statistical distribution of forces on the blocks. From (16.4) it is seen that the random force on a block is the sum of four random forces on the neighbor springs. These forces are not independent as one can see from (16.4) and the Gaussian distribution of forces on the block is

$$p(\bar{F}_{i,j}) = \frac{\exp\left(-\frac{\bar{F}_{i,j}^2}{32E}\right)}{4\sqrt{2\pi E}} \tag{16.10}$$

A block can slip if $|\bar{F}_{ij}| > 1$. Using (16.10) the probability that a block will be slipping P_s is

$$P_s(E) = 2\int_1^\infty \frac{\exp\left(-\frac{\bar{F}_{i,j}^2}{32E}\right)}{4\sqrt{2\pi E}}\, dF_{i,j} = \operatorname{erfc}\left(\frac{1}{\sqrt{32E}}\right) \tag{16.11}$$

We will show that our results satisfy this condition.

We have carried out a series of simulations on square arrays of up to 2000 × 2000 blocks. Springs on the boundaries of the array are attached to fixed walls. Random initial displacements were given to the blocks corresponding to specified values of E. Various initial distributions of energy (non-Gaussian) were used, and in all cases the system evolved to the Maxwell–Boltzmann distribution (16.8). A typical example is given in Figure 16.11 with $E = 1$. The statistical distribution of forces on the blocks was also determined and was found to be in excellent agreement with (16.10). The fraction of the blocks that are slipping P_s are given for several values of the mean energy E in Figure 16.12. Good agreement with the equilibrium prediction (16.11) is found.

As the fraction of slipping blocks increases with increasing values of E, a path of slipping blocks across the array is eventually established. This strongly resembles the percolation threshold for the site-percolation model considered in Chapter 15. Both are critical points and the critical value of E is 0.213 with the corresponding fraction of slipping blocks $P_s = 0.583$. This value can be compared with the critical point for the site percolation model where the probability that a lattice percolates is $p^* = 0.5927$. The small discrepancy between

the two values is attributed to correlations between blocks in the slider-block model. Figure 16.13 shows the frequency–size distribution at this critical point ($E = 0.213$) and, as a reference, the frequency–size distribution for the site-percolation model with $p = 0.5927$; the two distributions are virtually identical power laws. A typical slider-block configuration with a continuous path of slipping blocks across the array is shown in Figure 16.14. It is clearly very similar to the site-percolation distribution given in Figure 15.11(a).

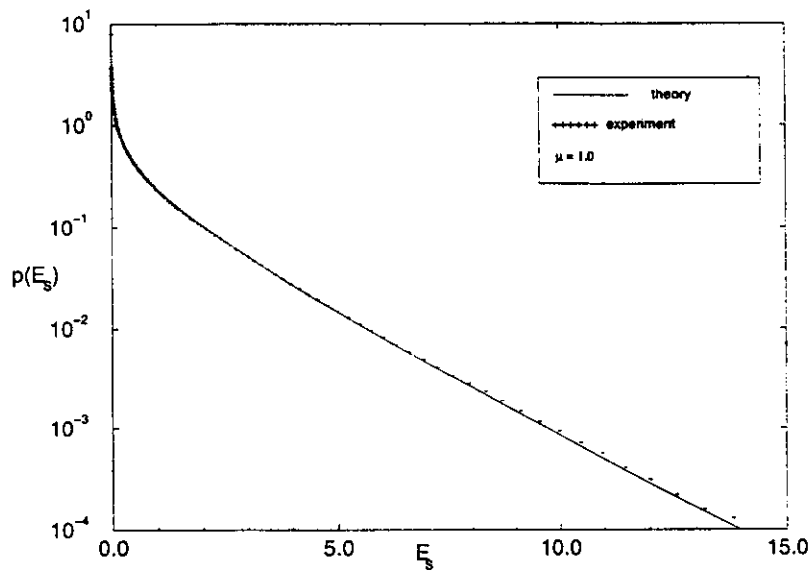

Figure 16.11. The probability distribution $p(\overline{E}_k)$ of the nondimensional energies $\overline{E}_k$ in the springs of a multiple slider-block model. The crosses are the result for a 2000 × 2000 array of slider blocks with $E = 1$. The solid line is the Maxwell–Boltzmann distribution of energies given in (16.8).

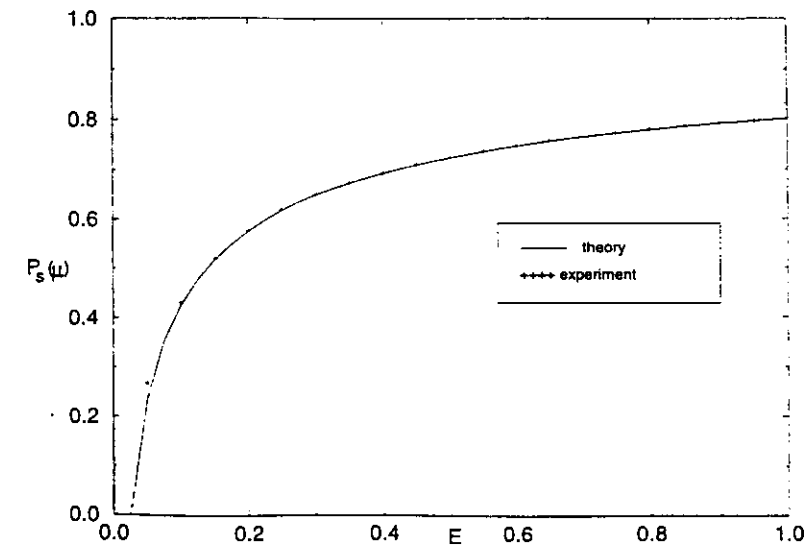

Figure 16.12. The fraction of the blocks that are slipping $P_s(E)$ is given as a function of the mean energy E. The crosses are results for a 1000 × 1000 array of slider blocks. and the solid line is the prediction from (16.11).

This simple energy-conserving system exhibits behavior that is quite similar to the seismicity in active tectonic regions such as California. In southern California the seismic activity level in the magnitude range $2 < M < 5$ not only satisfies the fractal Gutenberg–Richter frequency–magni-

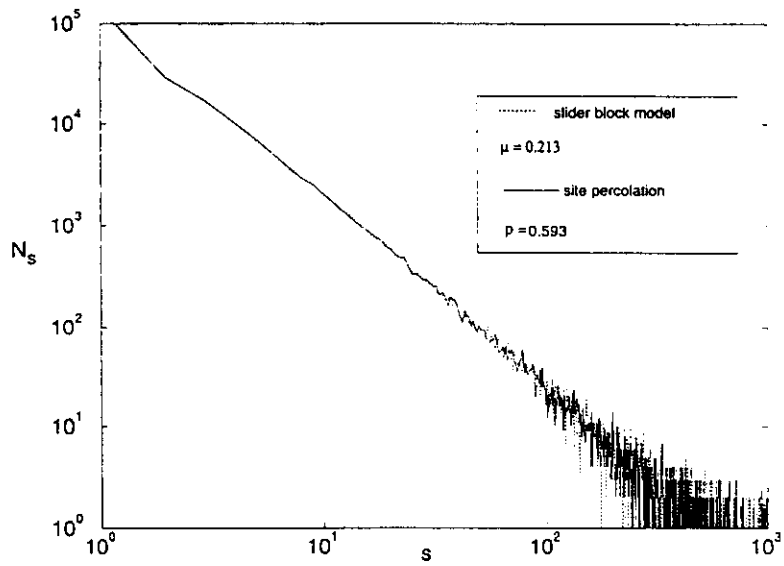

Figure 16.13. Number of clusters n_s of size s as a function of s. The solid line is the distribution of percolating clusters for a 2000×2000 array with the critical percolation probability $p = 0.5927$. The dashed line is the distribution of slipping clusters of blocks on our 2000×2000 array of slider blocks at the critical point $E = 0.213$.

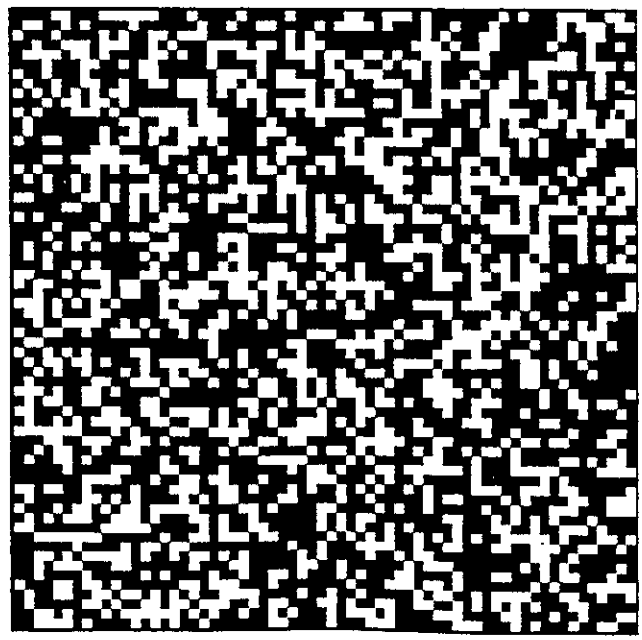

Figure 16.14. Illustration of a typical configuration of sliding blocks at the critical poin $E = 0.213$ for a 64×64 array. White blocks are stuck and black blocks are sliding. A continuous path of sliding blocks across the array is present.

tude scale, but also, the level of activity does not vary from year to year (see Figure 4.3). Earthquakes in this magnitude range strongly resemble the statistical fluctuations of the slider-block array near its critical point.

Further evidence supporting the applicability of the "percolation"-like model comes from the spatial distribution of seismicity in southern California. The distributions given in Figure 4.12 appear to correspond to the fractal dimension of the percolation "backbone" of a critical three-dimensional percolation cluster. It appears that the earthquakes on a complex array of faults form a connected path across the zone of crustal deformation in direct analogy to the "percolation backbone" of slipping blocks in the array. Rundle *et al.* (1995) found that the block energy distribution for a driven slider-block model is a Maxwell–Boltzmann distribution as the model approaches the mean field where fluctuations are minimal.

16.3 Forest-fire models

We next consider a class of models that are referred to as forest-fire models. These models generally exhibit self-organized criticality. We consider a square grid of sites, with each site designated by two numbers ij, where i is the row and j is the column. At each time step either a tree is randomly planted on a site or a match is dropped on the site. The sparking frequency f indicates how many trees are planted before a match is dropped. If $r = \frac{1}{100}$, 99 trees are planted (or are attempted to be planted) before a match is dropped. If a match is dropped on an empty site, nothing happens. But if a match is dropped on a tree, it ignites and all immediately adjacent trees burn.

As a specific example of our forest-fire model we consider the 10×10 grid illustrated in Figure 16.15. The model has been run for some time to establish a state of self-organized criticality and its initial state is given in Figure 16.15(a). We take $f = \frac{1}{5}$ so that four trees are planted before a match is dropped. Between Figures 16.15(a) and (b) there are 5 time steps and the randomly selected grid points were 71, 76, 56, 81, and 95. Trees were planted on 71, 56, and 81; 76 already had a tree, and a match was dropped on 95. This tree ignited and 35 adjacent trees also burned. Note that only trees immediately above, below, or to the sides of a burning tree also ignite. Following this forest fire 10 additional time steps are carried out to reach the distribution illustrated in Figure 16.15(c). The 10 randomly selected grid points are 72, 36, 00, 88, 08, 65, 44, 30, 45, and 44. Trees were planted on 72, 36, 88, 65, 44, 30, and 45; 00 already had a tree. The match dropped on 08 did not ignite because there was no tree on the grid point. The match dropped on 44 ignited this tree and burned the adjacent tree on 45. Following this small fire 25 additional time steps are carried out to reach the distribution illustrated in Figure 16.15(d). The 25 randomly selected grid points are

56, 36, 05, 15, 25, 68, 40, 52, 18, 81, 03, 79, 35, 35, 95, 56, 59, 80, 51, 07, 20, 56, 86, 46, and 30. Trees were already planted on 36, 05, 79, 35, 56, and 56. The matches dropped on 25, 81, 95, and 07 did not ignite because there were no trees on these grid points. The match dropped on 30 ignited this tree and burned six adjacent trees.

Frequency–size statistics for forest fires can be determined. Two examples for a 100 × 100 tree forest are given in Figure 16.16. The number of burning clusters N is given as a function of their size A_f for $f = \frac{1}{100}$ and $f = \frac{1}{2000}$. For the larger value $f = \frac{1}{100}$ fires consume the forest before large clusters can form. A reasonably good correlation with the fractal relation (2.2) is obtained taking $D = 2.00$. The roll-off from the power law near the larger end of the scaling region is very similar to that illustrated for the slider-block model in Figure 16.8. When the sparking frequency f is reduced to $\frac{1}{2000}$, we observe an excess number of catastrophic fires that consume all or nearly all of the 10,000 trees. Again this is very similar to the behavior found for slider blocks when the stiffness parameter is large as illustrated in Figure 16.9.

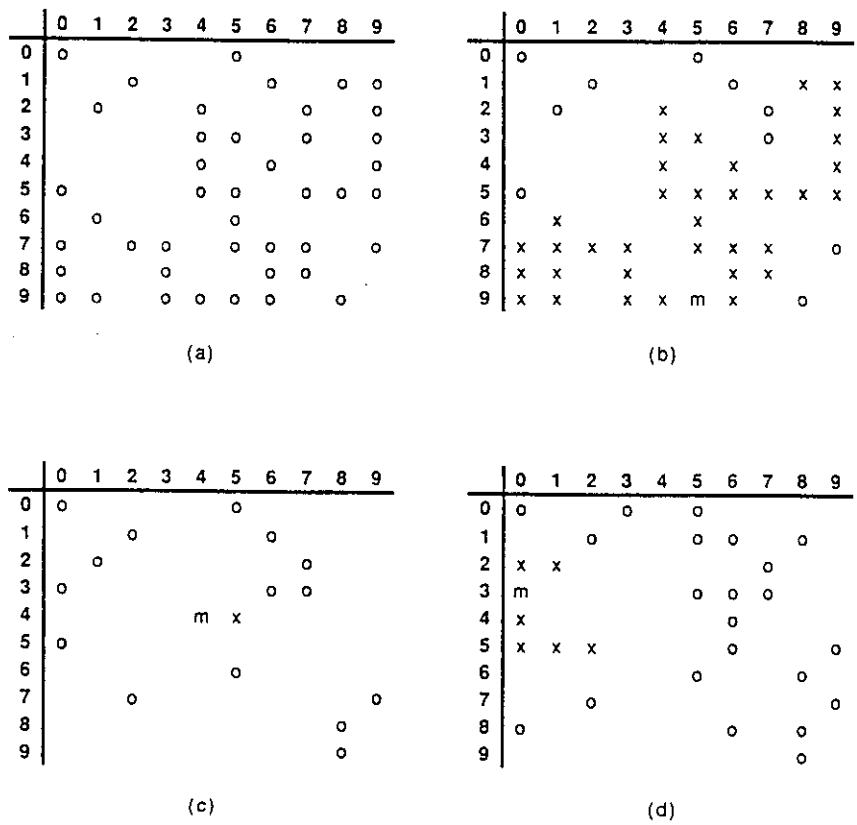

Figure 16.15. Illustration of the forest-fire model on a 10 × 10 grid of points. Each point is identified by its ij coordinates (i-row, j-column). We take $f = \frac{1}{5}$. (a) Grid points with trees are indicated by circles. Between (a) and (b) trees have been planted on points 71, 56, and 81; a match was then dropped on point 95, igniting the tree (indicated by m) and burning 35 adjacent trees (indicated by xs). Between (b) and (c) trees were planted on points 72, 36, 88, 65, 44, 31, and 45; a match was dropped on point 44, igniting this tree (indicated by m) and burning the adjacent tree at 45 (indicated by an x). Between (c) and (d) trees were planted on points 56, 15, 68, 40, 52, 18, 03, 35, 59, 80, 20, 86, and 46; a match was dropped on 30 (indicated by m) and burned 6 adjacent trees (indicated by xs).

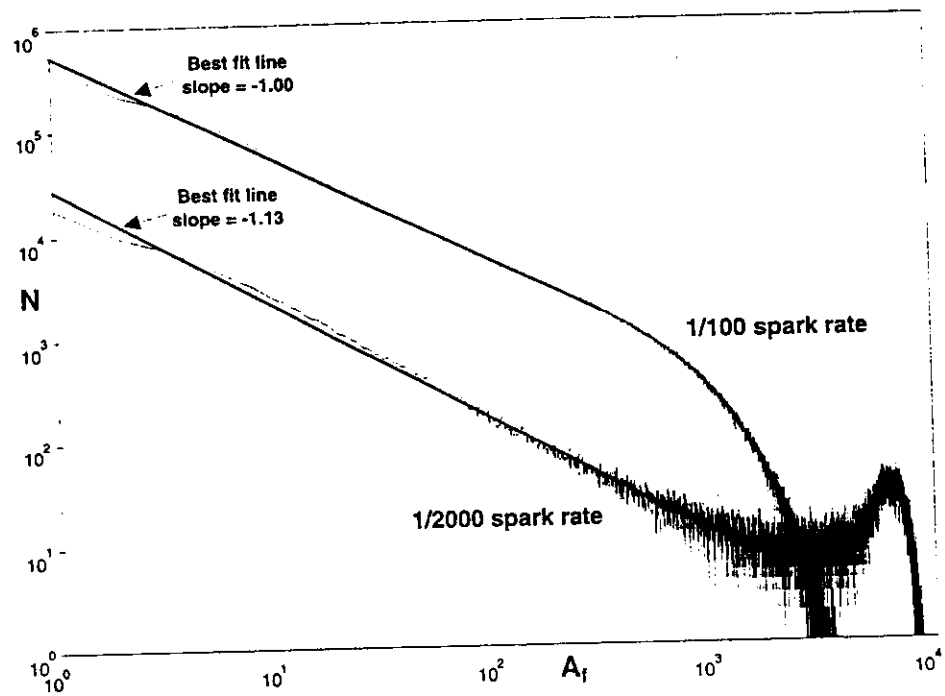

Figure 16.16. The number of forest fires N with size A_f (A_f is the number of trees that burn in a fire) is given as a function of A_f. Results are for a 100×100 forest grid with sparking parameters $f = \frac{1}{100}$ and $\frac{1}{2000}$.

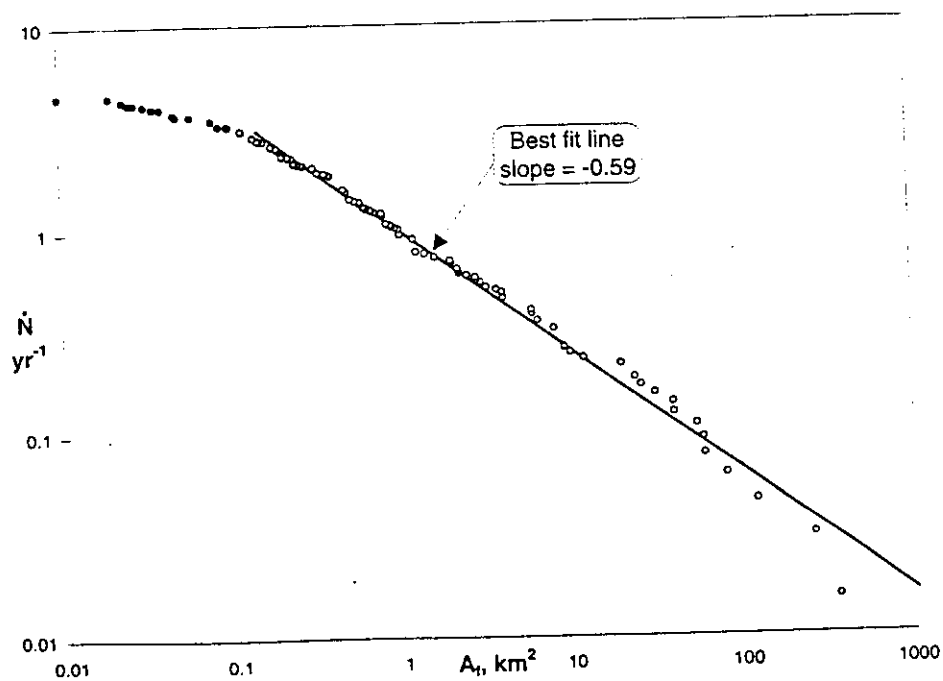

Figure 16.17. Cumulative number per year N of fires with burned areas greater than A_f given as a function of A_f. The data is for the Australian Capital Territory for the period 1926–1991. The best-fit straight line is with the fractal relation (2.6) taking $D = 1.18$.

It is also of interest to compare the results of forest-fire models with the frequency–size statistics for actual forest fires. Data for forest and brush fires in the Australian Capital Territory for the period 1926–1991 are given in Figure 16.17. A reasonably good straight-line fit with the fractal relation (2.6) is obtained taking $D = 1.18$. It should be emphasized that this is the cumulative number, whereas the model results given in Figure 16.16 are noncumulative.

The model results given in Figure 16.16 clearly illustrate the "Yellowstone Park" effect. After a massive forest fire covered a significant fraction of Yellowstone National Park, it was argued that if smaller fires had been allowed to burn, the massive forest fire could have been prevented. Allowing small fires to burn is equivalent to having a larger sparking frequency. The results given in Figure 16.16 illustrate how the small fires prevent the occurrence of catastrophic fires that burn essentially the entire model forest.

A variety of authors have studied forest-fire models, including Drossel and Schwabl (1992a, b, 1993a, b, 1994), Mosner *et al.* (1992), Bak *et al.* (1992), Drossel *et al.* (1993), Henley (1993), Christensen *et al.* (1993), and Clar *et al.* (1994), and Strocka *et al.* (1995). Johansen (1994) has applied the forest-fire model to the spread of diseases.

Problems

Problem 16.1. Consider the evolution of the cellular-automata model illustrated in Figure 16.1(b). (a) Which boxes have an additional particle in steps, 6, 7, 9 and 10? (b) Which boxes are unstable and how many particles are lost from the grid in steps 8, 11a, 11b, 11c, and 11d?

Problem 16.2. Consider the evolution of the cellular-automata model illustrated in Figure 16.1(b). (a) Which boxes have an additional particle in steps 12, 13, 14, and 15? (b) Which boxes are unstable and how many particles are lost from the grid in steps 16a, 16b, 16c, 16d, 17a, and 17b?

Problem 16.3. Consider the evolution of the cellular-automata model illustrated in Figure 16.1(b). (a) Which boxes have an additional particle in steps 18 and 19? (b) Which boxes are unstable and how many particles are lost from the grid in steps 20a, 20b, 20c, 20d, and 20e?

Problem 16.4.

1 2	433241332314342113212134323
3 4	
(*a*)	(*b*)

Consider a 2 × 2 grid of four boxes as illustrated above in (*a*). Also given above in (*b*) is a sequence of random numbers in the range 1–4.

Use the random numbers to assign particles to boxes and carry out the cellular automata model described in this chapter.

Problem 16.5.

1234

Consider the linear grid of four boxes illustrated above. Use the sequence of random numbers given in Problem 16.4 to assign particles to the four boxes. Use the following rules: When a box has two particles it is unstable and they are redistributed to the two adjacent boxes. If either of these boxes has two elements, they are again redistributed. Particles are lost from the ends of the linear grid.

Problem 16.6. Consider the evolution of the forest-fire model illustrated in Figure 16.15. Consider the configuration given in (d) and determine its subsequent evolution using the random number sequence 96, 09, 35, 67, 13, 33, 94, 44, 66, 37. (a) How many trees are planted? (b) How many forest fires occur and how many trees are burned in them?

Problem 16.7. Consider the evolution of the forest-fire model illustrated in Figure 16.15. Consider the configuration given in (d) and determine its subsequent evolution using the random number sequence 15, 81, 55, 25, 53, 65, 29, 17, 73, 56. (a) How many trees are planted? (b) How many forest fires occur and how many trees are burned in them?

Problem 16.8. Consider a linear (one-dimensional) forest-fire model using a grid of 10 points numbered sequentially from 0 to 9. Consider $p = 4$ so that after three trees are planted on random points, a match is dropped on a random point. Assume initially that trees are planted on points 1, 3, and 5 and consider the random sequence 0, 1, 7, 7, 3, 2, 6, 4, 0, 7, 7, 4, 9, 4, 7, 6. (a) Which points have trees after these 16 time steps? (b) How many forest fires occurred and how many trees burned in each fire?